JOURNAL OF SOLID STATE CHEMISTRY 118, 389–396 (1995)

Cationic Distribution in α-MZr_3F_{15} Series (M = Y, In, Ln, Tl)

J. P. Laval,*,[1] J. F. Gervais,† L. Fournès,† J. Grannec,† P. Gravereau,† A. Abaouz,‡ and A. Yacoubi‡

*Laboratoire des Matériaux Céramiques et Traitements de Surface, URA CNRS No. 320, Université de Limoges, 123 Avenue A. Thomas, 87060 Limoges Cedex, France; †Laboratoire de Chimie du Solide du CNRS, Université de Bordeaux I, 351 Cours de la Libération, 33405 Talence Cedex, France; and ‡Université Moulay Ismaïl, Faculté des Sciences, Meknès, Morocco

Received July 8, 1994; in revised form January 30, 1995; accepted January 31, 1995

A series of fluorozirconates MZr_3F_{15} was prepared by direct reaction of the binary fluorides, involving trivalent cations with a wide range of sizes: In, Tl, Lu, Yb, Y, Gd, Eu, and Pr (0.80 Å < R_{ion} < 1.13 Å). The samples were synthesized in sealed Pt tubes and heated between 700 and 1000°C, except for $TlZr_3F_{15}$, which was heated at 500°C under F_2 flow. Their crystal structure was solved by X-ray diffraction for single crystals of Y and Gd and for powders using the Rietveld method for the other phases. The structure is isotypic with that of $BiZr_3F_{15}$ and corresponds to a three-dimensional network of corner-sharing octahedra and dodecahedra, in a 1:3 proportion (cationic sites *6a* and *18e* of the $R\bar{3}c$ space group). The cationic distribution in these two sites depends on the size of the M^{3+} cation:

—Large cations, such as Y^{3+} and Ln^{3+}, are localized in the *18e* site, with Zr^{4+} distributed on both sites;

—a small cation, such as In^{3+}, is perfectly ordered in an octahedral site, with Zr^{4+} in a dodecahedral coordination;

—a cation of medium size, such as Tl^{3+}, presents an average distribution, with Zr^{4+} on both sites.

Structural relationships with anion-excess ReO_3-type and with the low-temperature polymorph β-$PrZr_3F_{15}$ are discussed.

INTRODUCTION

Since the characterization by Gaudreau in 1965 of a zirconium oxyfluoride, formulated as $ZrO_{0.67}F_{2.67}$ (1), the study of nonstoichiometric phases of structures derived from ReO_3-type by anion excess have increased significantly (2–5). This structure type is often observed in phases of composition (M, Zr)(O, F)$_{3+x}$ with M = Ca, Mg, transition metals, lanthanoides, ... Various types of cationic distributions are observed depending on the size or the charge of these M cations:

—Complete cationic disorder in cubic ($Pm\bar{3}m$; $a \approx 4$ Å) $ZrO_{0.67}F_{2.67}$ (6), $YbZrF_7$ (7), and $Yb_{0.2}Zr_{0.8}F_{3.2}O_{0.3}$ (8), and in $M_{1-x}Zr_xF_{2+2x}$ solid solutions involving divalent cations with small or medium size, such as Fe^{2+} or Ca^{2+} (5).

—Complete cationic ordering in $MZrF_6$ (M = Mg, Ca, Mn, Fe, Co, Ni, Zn) compounds, crystallizing either with a rhombohedral ($R\bar{3}$) or a cubic symmetry ($Fm\bar{3}m$; $a \approx 8$ Å) (5, 9). However, this cationic ordering does not prevent anionic excess, e.g., in $Ca_{1-x}Zr_xF_{2+2x}$ solid solution.

The excess of anions in these phases is accommodated by a simple substitution of some X corners in MX_6 octahedra by X–X edges, with the cationic coordination increasing from 6 to 7 or 8. The "anion-excess ReO_3-type" can be described as a three-dimensional network of corner-sharing MX_6 octahedra, MX_7 pentagonal bipyramids, and MX_8 dodecahedra.

The homogeneity domain and the stability of the cubic solid solutions increase when the size of the M^{3+} cation is close to that of the Zr^{4+} ionic radius (0.72 Å in sixfold coordination). With Ln^{3+} cations, such disordered phases are generally less stable. Several kinds of ternary fluorides involving a higher level of ordering are known:

—*Monoclinic $SmZrF_7$-type phases* (10), which are stable for all Ln cations and for Y. Their structure is built up of double layers associating, in a strictly ordered way, corner-sharing ZrF_6 octahedra and LnF_8 polyhedra. Extended solid solutions can be obtained with higher proportions of ZrF_4 but the mechanism of this nonstoichiometry has not yet been studied.

—*Orthorhombic $PrZr_2F_{11}$-type compounds* (11), strictly stoichiometric and stable only for Ln = La, Ce, Pr, and Nd. Their structure is closely related to β-ZrF_4-type, with Pr^{3+} located in square antiprisms and Zr^{4+} in monocapped trigonal prisms.

—*Rhombohedral ($R3m$ space group) β-$PrZr_3F_{15}$-type compounds* (12), also stoichiometric and obtained only for Ln = Pr and Nd at low temperature (T < 800°C). Their structure consists of a three-dimensional network of corner-sharing LnF_9 tricapped trigonal prisms and ZrF_7 pentagonal bipyramids. It is related to ReO_3-type by a simple mechanism, which will be detailed further.

In addition to the previous fluorides, *rhombohedral* ($R\bar{3}c$ space group) α-MZr_3F_{15} phases constitute the most extended group, isolated for all rare earths except La,

[1] To whom correspondence should be addressed.

0022-4596/95 $12.00

Ce, Pr, and Nd (13, 14), and also for M = Bi (15), In (16), U^{III} (17), Ti^{III} (16), and Tl^{III} (18). Homologous MM'_3F_{15} phases are known for M' = Hf with M = Sc (19) or Ln = Pr, Sm–Lu (14) and also for M' = Tb^{IV} with M = Sc (20) or Ln = Tb^{III}–Lu (20). The structure of $BiZr_3F_{15}$, as described by Caignol *et al.* (15), is composed of a three-dimensional network of corner-sharing MF_6 octahedra and MF_8 square antiprisms, in 1:3 proportion. It derives from the ReO_3 structure in the following way: In a group of eight corner-sharing octahedra viewed along a threefold axis ([111] direction of the ReO_3 structure), the substitution of edges for each of two adjacent corners of the six octahedra lying outside of the threefold axis creates six square antiprisms. The new cluster retains a threefold axis, which corresponds to the [001] direction of the $BiZr_3F_{15}$ structure. $BiZr_3F_{15}$ can then be considered as an anion-excess ReO_3 superstructure by ordered anionic insertion with the same mechanism as described by Papiernik and Frit (6) for disordered phases.

The cationic distribution in $BiZr_3F_{15}$ and also in YZr_3F_{15}, the structure of which was solved simultaneously but unpublished until now (21), exhibits peculiar features: Indeed, taking into account the presence in the $R\bar{3}c$ unit cell of two fully occupied 6*a* and 18*e* sites, it seemed reasonable, on the basis of the composition of the phase, to localize all Zr^{4+} cations on the 18*e* site and Bi^{3+} or Y^{3+} on the 6*a* site. In fact, in both phases, all Bi^{3+} and Y^{3+} cations occupy the 18*e* site, corresponding to a eightfold coordination (1/3 occupancy), and the Zr^{4+} ions are located at the same time on the 6*a* site (octahedra) and the 18*e* one (2/3 occupancy).

Considering the large variety in size and usual coordination of the M^{3+} cations able to associate with Zr^{4+} in this structural type (from Ti^{3+} to Pr^{3+} and Bi^{3+}), we decided to undertake a comparative structural study of numerous MZr_3F_{15} phases involving M trivalent cations that are the most different in size (M = Pr, Eu, Gd, Y, Yb, Lu, Tl and In), with an emphasis on the cationic ordering features.

EXPERIMENTAL

Preparation

All the phases were prepared by solid state reaction of the appropriate mixtures of ZrF_4 and MF_3 in sealed Pt tubes, for 1 day at 500°C (Tl), 700°C (In), and 850°C (Ln). For the thallium compound, the stoichiometric mixture was preheated at 500°C under a F_2 flow before annealing in a sealed tube (18). Single crystals of $GdZr_3F_{15}$ were obtained by heating at 1000°C in a sealed Pt tube and then cooling slowly to ambient temperature. Single crystals of YZr_3F_{15} were prepared at 700°C in a eutectic mixture of the BaF_2–YF_3–ZrF_4 system, melting at 550°C.

Density

The density of some of the phases prepared was determined by pycnometry or by hydrostatic pressure. The experimental values are in good agreement with the calculated ones, assuming six formulae per unit cell:

	$\rho_{exp.}$ (g · cm^{-3})	$\rho_{calc.}$ (g · cm^{-3})
$EuZr_3F_{15}$	4.62(3)	4.64
$GdZr_3F_{15}$	4.66(3)	4.67
YZr_3F_{15}	4.31(3)	4.32

Structure Determination

The observed intensities of $GdZr_3F_{15}$ and YZr_3F_{15} single crystals were respectively measured on a Nonius CAD4 and on a Siemens AED2* automatic diffractometers under the conditions noted in Table 1. The crystal structures were refined with the SHELX-76 program (22), using atomic scattering factors and anomalous dispersion corrections taken from the "International Tables for Crystallography" (23). The starting coordinates for cations were deduced from deconvolution of the Patterson function. The anionic sites were determined by Fourier-difference calculations. After refinement of the position parameters, anisotropic thermal vibration coefficients were introduced and refined. The introduction of a weighting scheme and of a secondary extinction parameter did not improve the result for YZr_3F_{15} but was significant for $GdZr_3F_{15}$. The final R factor converged to 0.036 for YZr_3F_{15} and to 0.024 for $GdZr_3F_{15}$.

The structures of the other phases were refined by the Rietveld method, with DBW 3.2S (24) or FullProf (25) refinement programs, starting with the structural model proposed by single crystal studies. The powder data were recorded either on a Philips PW1820 diffractometer or on a Siemens D5000 diffractometer, with either a graphite diffracted beam monochromator and a scintillation counter or a 14° Elphyse P.S.D. fast counter without a monochromator. This last device allows the simultaneous recording of a 14° angular range and therefore a lower recording time (typically 2–4 hr for $15° \leq 2\theta \leq 130°$), but can only be used in the absence of fluorescence and when peak overlapping does not induce trouble because of the lower angular resolution. The recording and refinement parameters for the powder samples are gathered in Table 2. The refined atomic parameters were the same as for single crystal studies but only isotropic thermal factors were used. For most structures, the respective proportions of Zr and M on both cationic sites were refined.

The structural parameters are reported in Tables 3a and 3b and the main interatomic distances in Table 4. Results for $TlZr_3F_{15}$ are taken from Ref. (18).

TABLE 1
Recording Characteristics for Single Crystal Determinations

	YZr_3F_{15}	$GdZr_3F_{15}$
Cell parameters (Å)	a = 12.384(6)	a = 12.463(1)
	c = 11.270(5)	c = 11.335(1)
V (Å^3)	1496.84	1524.74
Symmetry	Rhombohedral ($R\bar{3}c$)	Rhombohedral ($R\bar{3}c$)
Z	6	6
Crystal size (mm)	R = 0.08	0.19 × 0.16 × 0.03
Transmission factor	—	$0.474 < T < 0.998$
Absorption factor μ (mm^{-1})	9.0	9.6
	$0 \le h \le +26$	$-22 \le h \le +22$
hkl limits	$0 \le k \le +26$	$-22 \le k \le +22$
	$0 \le l \le +23$	$-20 \le l \le +20$
Diffractometer	Siemens AED-2	Nonius CAD-4
Recording mode	ω-2θ	ω-2θ
Wavelength	Mo$K\alpha$	Mo$K\alpha$
Monochromator	Graphite	Graphite
Number of exp. reflections	3687	12530
Number of independent reflections	1233	995
	($I/\sigma(I) > 4$)	($I/\sigma(I) > 3$)
Number of refined parameters	32	33
Weighting scheme	—	$1/\sigma^2(F_0)$
Secondary extinction parameter	—	$24(1) \times 10^{-5}$
R	0.036	0.024
R_w	0.036	0.019

STRUCTURE DESCRIPTION

A. YZr_3F_{15} and $GdZr_3F_{15}$

The projection of the structure of YZr_3F_{15} onto the xy plane is represented in Fig. 1. The structures of both phases are exactly the same, as attested by the closeness of the structure parameters of Table 3. They are constituted, as is $BiZr_3F_{15}$, of a three-dimensional network of corner-sharing MF_6 octahedra and of MF_8 polyhedra, which, in fact, appear closer to dodecahedra than to square antiprisms (Fig. 2). The cationic distribution on the 6*a* and 18*e* cationic sites could not be precisely determined for YZr_3F_{15} because of the isoelectronic character of Y and Zr. In $GdZr_3F_{15}$, the great difference between

TABLE 2
Recording and Refinement Parameters from Powders

	Pr	Eu	Yb	Lu	In
Cell parameters (Å)	12.5335(2)	12.461(1)	12.3466(2)	12.3305(2)	12.1045(2)
	11.4269(2)	11.344(1)	11.2288(2)	11.2161(2)	11.0980(2)
Recording limits (° 2θ)	15–130	10–110	18–130	18–130	15–130
Scan step (° 2θ)	0.04	0.02	0.029	0.029	0.04
Zero shift (° 2θ)	−0.0001(4)	0.0464(11)	0.0157(4)	0.0234(4)	0.1763(4)
Recording equipment	[a]	[b]	[c]	[c]	[a]
Refinement program	FullProf	DBW3.2S	FullProf	FullProf	FullProf
Profile function	ps-Voigt	ps-Voigt	ps-Voigt	ps-Voigt	ps-Voigt
R_B	7.6	7.8	5.0	4.7	5.3
R_P	7.6	13.3	1.5	1.6	6.6
R_{WP}	9.8	17.4	2.0	2.1	8.6

[a] Siemens D5000 diffractometer + scintillation counter + graphite back monochromator; recording time, 72 hr.

[b] Philips PW1820 diffractometer + graphite back monochromator + scintillation counter; recording time, 56 hr.

[c] Siemens D5000 diffractometer + Elphyse 14° P.S.D. counter—no monochromator; recording time, 5 hr.

TABLE 3a
Refined Structure Parameters

Site	Atom	Parameter	Pr	Eu	Gd	Y	Yb	Lu	Tl	In
6*a*	*M*/Zr	n*M*	0.	0.	0.	0.	0.	0.	0.124(1)	0.161(5)
		nZr	0.167	0.167	0.167	0.167	0.167	0.167	0.043(1)	0.006(5)
		B (Å²)	0.57(6)	0.90(1)	0.52(1)	0.39(1)	0.81(5)	0.83(4)	0.83(5)	0.20(4)
18*e*	*M*/Zr	*x*	0.4288(2)	0.4272(2)	0.4279(1)	0.42743(3)	0.4279(1)	0.4279(1)	0.429(1)	0.4307(1)
		n*M*	0.167	0.167	0.167	0.167	0.167	0.167	0.043(1)	−0.001(13)
		nZr	0.333	0.333	0.333	0.333	0.333	0.333	0.457(1)	0.501(13)
		B (Å²)	0.74(3)	0.88(5)	0.441(6)	0.29(1)	0.99(2)	0.75(2)	0.98(4)	0.20(2)
18*e*	F(1)	*x*	0.7145(9)	0.717(2)	0.7140(2)	0.7140(3)	0.7144(5)	0.7158(4)	0.709(1)	0.7106(6)
		B (Å²)	1.8(2)	2.2(2)	1.61(7)	1.26(8)	0.7(1)	1.0(1)	1.5(2)	0.7(1)
36*f*	F(2)	*x*	0.2605(6)	0.2548(8)	0.2547(1)	0.2544(2)	0.2526(4)	0.2516(4)	0.253(1)	0.2518(4)
		y	0.5220(5)	0.5192(8)	0.5151(1)	0.5142(2)	0.5112(4)	0.5115(4)	0.508(1)	0.5093(4)
		z	0.0150(7)	0.016(1)	0.0194(1)	0.0210(2)	0.0215(5)	0.0204(5)	0.030(1)	0.0267(3)
		B (Å²)	0.6(2)	2.2(2)	1.38(5)	1.20(6)	1.8(1)	1.3(1)	0.6(2)	0.4(1)
36*f*	F(3)	*x*	0.2765(6)	0.2747(7)	0.2778(2)	0.2786(2)	0.2761(4)	0.2766(4)	0.287(1)	0.2826(4)
		y	0.0890(5)	0.0878(8)	0.0899(2)	0.0896(2)	0.0878(3)	0.0896(3)	0.092(1)	0.0893(4)
		z	0.5361(6)	0.5389(7)	0.5375(1)	0.5381(2)	0.5362(4)	0.5381(4)	0.538(1)	0.5413(4)
		B (Å²)	1.6(2)	2.2(2)	1.49(6)	1.17(6)	1.9(1)	1.6(1)	0.8(2)	0.6(1)

the cationic scattering factors allows the cationic distribution on both sites to be refined without any ambiguity, as in $BiZr_3F_{15}$: all Gd^{3+} cations (6 per cell) are located on the 18*e* site (eightfold coordination) and Zr^{4+} cations (18 per cell) are divided up between the 6*e* site that they entirely fill and the 18*e* site, which is statistically occupied by 12 Zr^{4+} and 6 Gd^{3+}. The unit cell is then composed of 6 ZrF_6 octahedra, 6 GdF_8 dodecahedra, and 12 ZrF_8 dodecahedra. The Zr–F(2) distances in the octahedron are logically very close (2.014 Å in YZr_3F_{15} and 2.005 Å in $GdZr_3F_{15}$) and are in good agreement with those generally encountered (1.98–2.02 Å). The Zr/*M*–F distances give evidence of a hybrid character but are closer to the usual Zr–F bonds in eightfold coordination, which expresses the dominant proportion of Zr^{4+} in the 18*e* site. In order to determine if Y^{3+} and Zr^{4+} are distributed in the same way in YZr_3F_{15}, the fluorescence of Eu^{3+} in the doped phase, $Y_{0.99}Eu_{0.01}Zr_3F_{15}$, was studied under exactly the same conditions as used for $Bi_{0.99}Eu_{0.01}Zr_3F_{15}$ by Caignol *et al.* (15). The emission spectrum of the $^5D_0 \rightarrow {}^7F_J$ transitions, quite identical to the spectrum of the quoted phase, is in good agreement with the *C*2 local symmetry of the 18*e* site, which confirms that the above three phases have exactly the same cationic distribution.

TABLE 3b
Anisotropic Temperature Factors for $GdZr_3F_{15}$ and YZr_3F_{15} (U × 10^4)

	U_{11}	U_{22}	U_{33}	U_{23}	U_{13}	U_{12}
⟨$GdZr_3F_{15}$⟩						
Zr (6*a* site)	56(1)	56(1)	84(2)	0	0	28(1)
Gd/Zr (18*e* site)	58(1)	67(1)	46(1)	2(1)	1	34(1)
F(1)	187(7)	262(11)	188(9)	−65(9)	−32(4)	131(6)
F(2)	188(7)	133(6)	203(6)	61(5)	53(5)	81(5)
F(3)	195(7)	210(7)	163(6)	32(5)	−3(5)	102(6)
⟨YZr_3F_{15}⟩						
Zr (6*a* site)	43(1)	43(1)	63(2)	0	0	21(1)
Y/Zr (18*e* site)	35(1)	44(1)	32(1)	1(1)	1	22(1)
F(1)	166(8)	168(12)	146(10)	−48(9)	−24(5)	84(6)
F(2)	160(8)	115(7)	181(8)	63(6)	54(7)	76(7)
F(3)	174(9)	139(8)	131(7)	−15(6)	1(6)	66(7)

TABLE 4
Main Interatomic Distances

	Pr	Eu	Gd	Y	Yb	Lu	Tl	In
Zr/M–F(2) × 6	1.932(8)	1.948(6)	2.005(6)	2.014(2)	2.037(5)	2.025(5)	2.100(6)	2.053(4)
Zr/M–F(1) × 2	2.168(5)	2.145(4)	2.146(4)	2.132(1)	2.127(3)	2.125(3)	2.119(4)	2.113(3)
Zr/M–F(2) × 2	2.368(6)	2.356(7)	2.287(7)	2.264(2)	2.227(5)	2.233(5)	2.132(7)	2.136(4)
Zr/M–F(3) × 2	2.279(8)	2.156(6)	2.159(6)	2.136(2)	2.127(4)	2.136(4)	2.120(6)	2.090(5)
Zr/M–F(3) × 2	2.127(7)	2.140(6)	2.122(6)	2.124(2)	2.111(5)	2.110(5)	2.073(6)	2.086(5)

B. Cationic Distribution in α-MZr_3F_{15} Series (M = Pr, Eu, Yb, Lu, Tl, In)

The study of cationic distribution in α-MZr_3F_{15} series was extended to M^{3+} larger cations, such as Pr^{3+} and Eu^{3+}, and to smaller cations (Yb^{3+}, Tl^{3+}, Lu^{3+}, In^{3+}). For $PrZr_3F_{15}$ (previously unknown but easily prepared at 850°C) and $EuZr_3F_{15}$, the positions and the cationic distribution are exactly the same as for the previous phases. For $EuZr_3F_{15}$, a Mössbauer spectrum was recorded. It consists of a singlet with an isomeric shift of 0.132 mm · sec^{-1}. This value is close to that measured for ^{151}Eu in $EuSnF_7$ and characterizes trivalent europium (26). The Mössbauer analysis is consistent with the localization of europium in only one site and thus confirms the cationic distribution.

Whatever the ionic radius, the same behavior is encountered in all *Ln* fluorozirconates, since Zr^{4+} is located in both cationic sites and Ln^{3+} exhibits an eightfold coordination. This result is not completely unexpected because if e.g., Lu^{3+} and Yb^{3+} easily accept sixfold and sevenfold coordination, their ionic radii are nevertheless larger than that of Zr^{4+}.

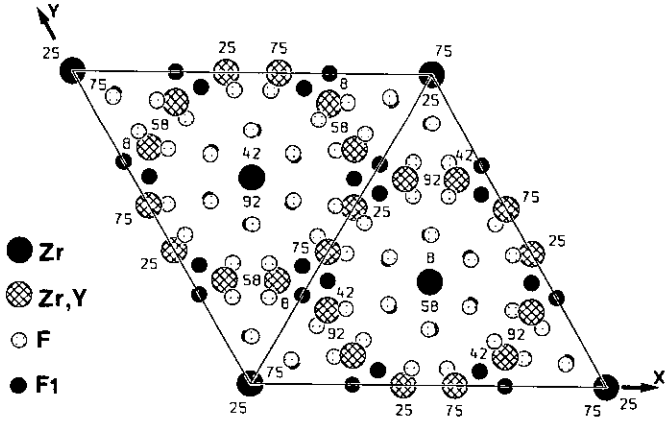

FIG. 1. Projection of the YZr_3F_{15} structure onto the *xy* plane. In all drawings concerning this phase, large dark circles represent M cations in 6*a* site (sixfold coordinated), squared circles represent M' cations in the 18*e* site (eightfold coordinated), and small dark circles represent F(1) bridging anions.

For Tl and In fluorozirconates, a drastic change in cationic distribution is clearly observed: in $TlZr_3F_{15}$, about 3/4 of the octahedral site is occupied by Tl^{3+} cations and 92% of the dodecahedral site by Zr^{4+}. For the slightly smaller In^{3+} cation, the inversion of distribution is complete and a cationic ordering appears with all In^{3+} in the 6*a* site and all Zr^{4+} in the 18*e* one. $InZr_3F_{15}$ is then the only completely ordered phase of the MZr_3F_{15} series. It is interesting to note that, in spite of its slightly smaller size, the Zr^{4+} cation is more stable in eightfold coordination than In^{3+}. Such a feature is probably related to the higher charge of zirconium. In $InZr_3F_{15}$, the In–F bond (2.053 Å) is longer than previous Zr–F bonds in sixfold coordination and the average ⟨Zr–F⟩ distance (2.106 Å) fits the values generally observed in eightfold coordination very well.

C. Structural Relationships between ReO_3, α- and β-MZr_3F_{15} Types

As previously described (15), the α-MZr_3F_{15} structure corresponds to an anion-excess ReO_3 superstructure with a threefold axis of the ReO_3 subcell colinear with the [001] direction of the hexagonal MZr_3F_{15} unit cell. In this description, the excess of anions is introduced in the ReO_3 ccp structure by substituting in an ordered way F–F edges for F corners in MF_6 octahedra, transforming them into MF_8 dodecahedra. Each unmodified octahedron shares F(2) corners with six dodecahedra and each dodecahedron is connected to six other dodecahedra and two octahedra.

As ReO_3, this structure can also be described as a stacking of identical layers but in which three-quarters of the octahedra are replaced by dodecahedra (Fig. 3). The structural formula then becomes "MZr_3F_{12}" + 3F ⇒ MZr_3F_{15}. In fact, the F(1) excess anions do not really form F–F pairs between adjacent cations as in disordered anion-excess phases, but *bridge* cations located on *opposite* corners of a "ReO_3" square face, shortening the cation–cation distance (e.g., from about $4.1\sqrt{2}$ Å to 4.264 Å for YZr_3F_{15}) and transforming this square face into two triangular ones. This bridging mechanism is repeated in two successive layers in such a way that a ReO_3 cube is

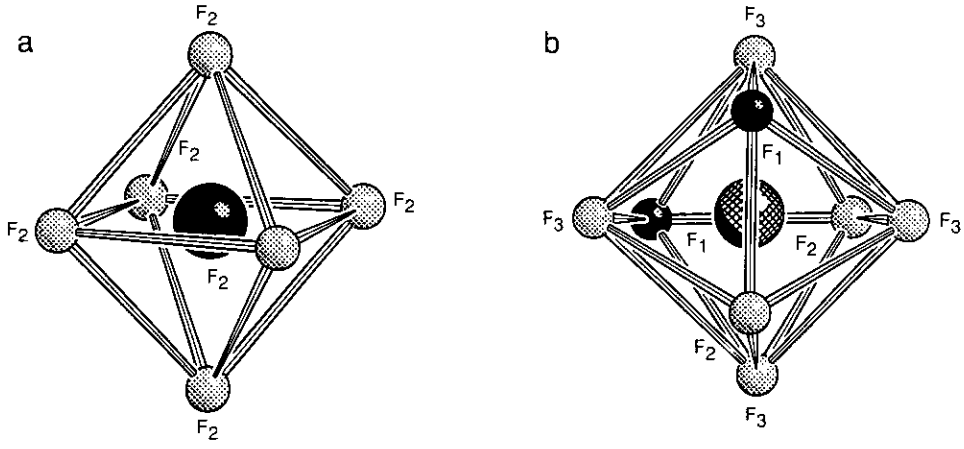

FIG. 2. (a) MF_6 octahedron; (b) $M'F_8$ dodecahedron.

transformed into two trigonal prisms, as shown in Fig. 4. The insertion of the F(1) excess anions occurs twice for each affected octahedron, which corresponds to replacing two opposite F corners by F(1)–F(2) edges, creating the dodecahedron represented in Fig. 2. The developed structural formula can then be written

$$24\ MF_3 + 18\ F(1) \Rightarrow M_6M'_{18}F(1)_{18}F(2)_{36}F(3)_{36},$$

where F(1) is excess anion, F(2) and F(3) are ReO_3-type anions, M is a cation in sixfold coordination, and M' is a cation in eightfold coordination.

The regular bridging process changes the 4^4 cationic plane net into a $[3.4^3][3^2.4^3]$ net (in Schläffli notation), represented in Fig. 5, which itself derives from a semi-regular $3^2.4.3.4$ plane net, intermediate between a square 4^4 net and a hexagonal 3^6 one (27). The presence of such $[3.4^3][3^2.4^3]$ nets in the α-MZr_3F_{15} type easily allows one to relate this structure type to the β variety (12), which is also based on the stacking of the same identical cationic plane nets (Fig. 6). Therefore, both structures derive from the ReO_3-type by the same anionic bridging mechanism. The main difference between them lies in the relative arrangement, from one layer to another, of the anionic bridging:

—In the α-form, each dodecahedron shares two F(1) anions with the dodecahedra of opposite square faces, transforming these faces into triangular ones, as already shown. The relative distribution of these triangular faces between adjacent layers creates the trigonal prisms of Fig. 4.

—In the β form, each LnF_9 tricapped trigonal prism shares three F(3) bridging anions of three adjacent square faces, giving rise to the distorted ReO_3 subcell represented in Fig. 7.

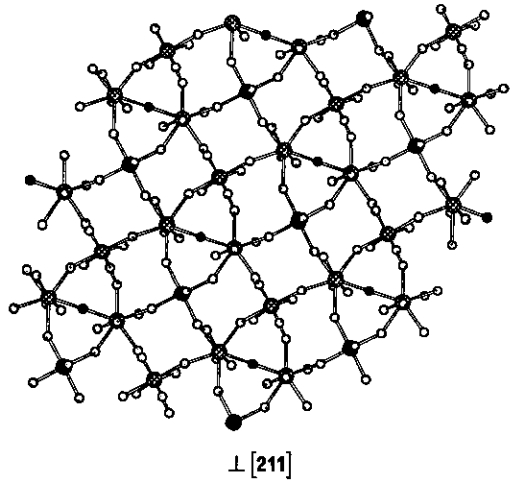

FIG. 3. Representation of a layer (perpendicular to a [211] direction) of corner-sharing MF_6 and $M'F_8$ polyhedra in an α-MZr_3F_{15} structure.

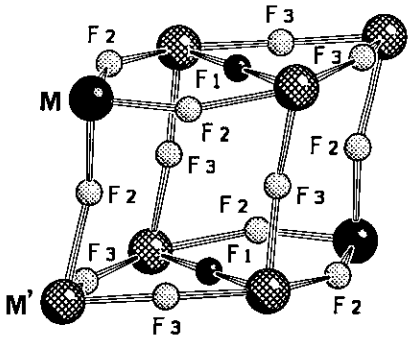

FIG. 4. Transformation of a ReO_3 cube in two trigonal prisms by F(1) bridging through square faces in two successive layers of a α-MZr_3F_{15} structure.

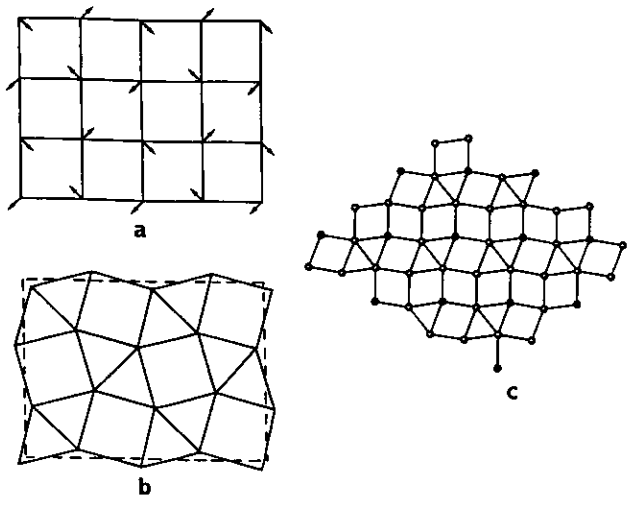

FIG. 5. Structural mechanism of plane net transformation from a 4^4 square plane net (a) to a $[3.4^3][3^2.4^3]$ one (in Schlaffli notation) (c), itself deriving from a semiregular $3^2.4.3.4$ plane net (b).

The different distribution of the bridged faces in both structures is responsible for the difference in unit cells and space groups: If a_{hex} parameters are very close ($\approx$ 12 Å), c_{hex} is approximately doubled in the α variety; the space groups are, respectively, $R3m$ and $R\bar{3}c$ in the β and α phases. Moreover, in the β form, all cations are affected by bridging whereas in the α- form some octahedra remain unchanged.

It is possible to derive these two phases with the same composition from the ReO_3-type by a different spatial distribution of the same "defect," generating polyhedra of various coordination, according to the structural equations

$$ZrF_{6/2} + 2\ ZrF_{8/2} + MF_{8/2} \Rightarrow MZr_3F_{15} \quad (\alpha\text{-variety})$$
$$MX_3 + 2MX_4 + MX_4 \Rightarrow M_4X_{15}$$

and

$$3\ ZrF_{7/2} + MF_{9/2} \Rightarrow MZr_3F_{15} \quad (\beta\text{-variety})$$
$$3MX_{3.5} + MX_{4.5} \Rightarrow M_4X_{15}.$$

The α type, containing Ln^{3+} in eightfold coordination, is more stable for the smaller Ln^{3+} cations whereas the β type, with ninefold coordination, is more suitable for larger ones (Pr, Nd).

CONCLUSION

The structural determination of various phases belonging to the α-MZr$_3$F$_{15}$-type shows that this structure type exhibits an interesting evolution of the cationic ordering with the trivalent cation size, which fully explains that a large variety of M^{3+} cations can be associated to Zr^{4+}, Hf^{4+}, and Tb^{4+} in this series. The only completely ordered phase is $InZr_3F_{15}$, in which In^{3+} exhibits the octahedral coordination (6*a* site) and Zr^{4+} the dodecahedral coordination (18*e* site). For all $LnZr_3F_{15}$ compounds, the 6*a* site is only occupied by Zr^{4+} whereas the 18*e* site contains a mixture of Zr^{4+} and Ln^{3+}. $TlZr_3F_{15}$ is the most disordered phase, with Tl^{3+} and Zr^{4+} cations distributed on both sites. Although their structure was not determined, it is suggested that $TiZr_3F_{15}$ and probably

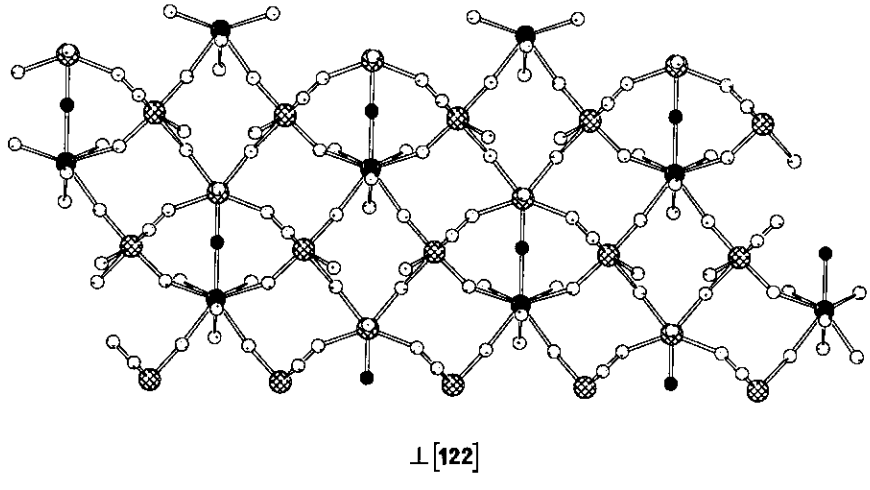

FIG. 6. β-MZr$_3$F$_{15}$ layer (perpendicular to a [122] direction). The cationic plane net is the same as in the α-MZr$_3$F$_{15}$-type (Fig. 3), in spite of the different nature of the polyhedra. Large dark circles represent Pr^{3+} in 3*a* site (ninefold coordinated), squared circles represent Zr^{4+} in 9*b* site (sevenfold coordinated) and small dark circles, F(3) bridging anions.

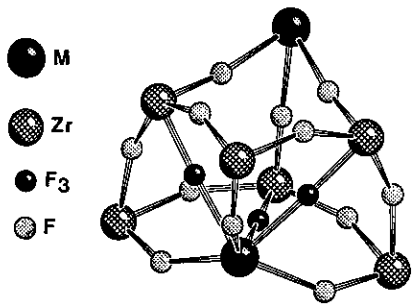

FIG. 7. Distorted ReO_3 subcell in β-MZr_3F_{15} type (compared to Fig. 4). Large dark circles represent Pr^{3+} in 3*a* site (ninefold coordinated), squared circles represent Zr^{4+} in 9*b* site (sevenfold coordinated) and small dark circles represent F(3) bridging anions.

$ScHf_3F_{15}$ and $ScTb_3F_{15}$ are also fully ordered, as is $InZr_3F_{15}$.

The α- and β-MZr_3F_{15} varieties are closely related to the ReO_3-type by an original mechanism of anion excess accommodation by F bridging through ReO_3 square faces. Both types are closely related and mainly differ by their cationic coordination: 6 + 8 for α, and 7 + 9 for β, resulting from a different distribution of the same structural "defect."

The α-MZr_3F_{15}-type appears, considering the more-or-less extensive cationic disorder described in the present paper, as an intermediate structure type between ReO_{3+x} solid solutions and well-defined compounds like $PrZr_2F_{11}$ and β-MZr_3F_{15}.

ACKNOWLEDGMENTS

The authors thank Pr M. Leblanc, of Le Mans University, for the recording of a single crystal of YZr_3F_{15} and Pr D. Avignant, of Clermont-Ferrand University, for the optical study of Eu-doped YZr_3F_{15}.

REFERENCES

1. B. Gaudreau, *Rev. Chim. Miner.* **2,** 1 (1965).
2. M. Poulain, M. Poulain, and J. Lucas, *Mater. Res. Bull.* **7,** 319 (1972).
3. M. Poulain, M. Poulain, and J. Lucas, *C. R. Acad. Sci. C* 276, 1553 (1973).
4. M. Poulain, M. Poulain, and J. Lucas, *Rev. Chim. Miner.* **12,** 9 (1975).
5. J. Grannec, A. Yacoubi, L. Fournès, A. Tressaud, and P. Hagenmuller, *J. Solid State Chem.* **70,** 323 (1987).
6. R. Papiernik and B. Frit, *Mater. Res. Bull.* **19,** 509 (1984).
7. M. Poulain and B. C. Tofield, *J. Solid State Chem.* **39,** 314 (1981).
8. B. C. Tofield, M. Poulain, and J. Lucas, *J. Solid State Chem.* **27,** 163 (1979).
9. D. Babel and A. Tressaud, "Inorganic Solid Fluorides" (P. Hagenmuller, Ed.), Chap. 3, Academic Press. San Diego, 1985.
10. M. Poulain, M. Poulain, and J. Lucas, *J. Solid State Chem.* **8,** 132 (1973).
11. J. P. Laval and A. Abaouz, *J. Solid State Chem.* **100,** 90 (1992).
12. J. P. Laval and A. Abaouz, *J. Solid State Chem.* **96,** 324 (1992).
13. A. I. Popov, M. D. Valkovskii, P. P. Fedorov, and Yu.M. Kiselev, Zh. Neorg. Khim. **36**(4), 842 (1991).
14. Yu.M. Korenev, P. I. Antipov, and A. V. Novoselova, *Zh. Neorg. Khim.* **25,** 1255 (1980).
15. E. Caignol, J. Metin, R. Chevalier, J. C. Cousseins, and D. Avignant, *Eur. J. Solid State Inorg. Chem.* **25,** 399 (1988).
16. J. C. Champarnaud-Mesjard, J. P. Laval, and B. Gaudreau, *Rev. Chim. Miner.* **11,** 735 (1974).
17. G. Fonteneau and J. Lucas, *J. Inorg. Nucl. Chem.* **36,** 1515 (1974).
18. J. F. Gervais, L. Fournès, J. Grannec, P. Gravereau, J. P. Laval, and P. Hagenmuller, *Mater. Res. Bull.* **29**(4), 405 (1994).
19. P. P. Fedorov, O. V. Pil'Gun, B. P. Sobolev, and P. I. Fedorov, *Zh. Neorg. Khim.* **35**(4), 1068 (1990).
20. M. N. Brechovski, A. I. Popov, Yu.M. Kiselev, A. L. Plinskii, and V. A. Fedorov, *Zh. Neorg. Khim.* **34**(4), 1021 (1989).
21. J. P. Laval, private communication.
22. G. M. Sheldrick, "SHELX-76, Program for Crystal Structure Determination." Cambridge University, 1976.
23. "International Tables For X-Ray Crystallography." Kynoch Press, Birmingham, 1968.
24. D. B. Wiles and R. A. Young, *J. Appl. Crystallogr.* **14,** 149 (1981).
25. J. Rodriguez-Carvajal, "FullProf," Institut Max von Laüe–Paul Langevin (ILL), Grenoble, 1990.
26. J. Grannec, P. Lagassie, and L. Fournès, *Mater. Lett.* **9,** 33 (1989).
27. M. O'Keeffe and B. G. Hyde, *Philos. Trans. R. Soc. London A* **295,** 553 (1980).